

A new nonlinear vortex state in square-duct flow

S. OKINO¹, M. NAGATA¹†, H. WEDIN² AND A. BOTTARO²

¹Department of Aeronautics and Astronautics, Graduate School of Engineering,
Kyoto University, Kyoto 606-8501, Japan

²Dipartimento di Ingegneria, delle Costruzioni, dell'Ambiente e del Territorio,
University of Genova, Via Montallegro 1, 16145 Genoa, Italy

(Received 6 November 2009; revised 13 May 2010; accepted 13 May 2010;
first published online 1 July 2010)

A new nonlinear travelling-wave solution for a flow through an isothermal square duct is discovered. The solution is found by a continuation approach in parameter space, starting from a case where the fluid is heated internally. The Reynolds number for which the travelling wave emerges is much lower than that of the solutions discovered recently by an analysis based on the self-sustaining process (Wedin *et al.*, *Phys. Rev. E*, vol. 79, 2009, p. 065305; Uhlmann *et al.*, *Advances in Turbulence XII*, 2009, pp. 585–588). Furthermore, the new travelling-wave solution is shown to be unstable from the onset.

Key words: bifurcation, nonlinear instability, transition to turbulence

1. Introduction

Transition to turbulence in canonical unidirectional shear flows is still an unsolved problem in fluid mechanics since the pioneering experimental study on pipe flow by Osborne Reynolds in 1883. The difficulty consists in extracting relevant information from the Navier–Stokes equations to understand what is observed in real-life turbulence.

The laminar flow through isothermal square ducts and circular pipes is asymptotically stable to small disturbances (Davey & Drazin 1969; Tatsumi & Yoshimura 1990). Hence to cause a shift from a laminar to a turbulent state for these flow cases a finite-amplitude disturbance is necessary, and the threshold amplitude is a function of the disturbance shape. Such a disturbance is also sufficient if it sits in phase space on an ‘outer’ unstable manifold (‘outer’ meaning that it faces the turbulent attractor) of the laminar–turbulent boundary, defined as the boundary separating the basin of attraction of the laminar flow from that of turbulence. The experimental work by Darbyshire & Mullin (1995) on pipe flow demonstrates that the required finite-amplitude disturbance ϵ to initiate the transition to turbulence in circular pipe flow, scales like Re^{-1} – same scaling is reported in the experiments by Hof, Juel & Mullin (2003) in the range $2000 \leq Re \leq 20\,000$. This has also been theoretically recovered by Gavarini, Bottaro & Nieuwstadt (2005) on the same flow configuration. Likewise, Chapman (2002) postulates two scenarios of turbulence breakdown for plane Couette flow (PCF) and plane Poiseuille flow using asymptotic analysis of the Navier–Stokes equations. Therein it is found that ϵ scales in the interval $Re^{-1.5} \leq \epsilon \leq Re^{-1}$ depending on the postulated transition scenario and flow

† Email address for correspondence: nagata@kuaero.kyoto-u.ac.jp

configuration. A similar result is obtained by Waleffe & Wang (2005) on PCF where the smallest disturbance amplitude needed to trigger transition scales as Re^{-1} .

The turbulent state is thought to be described by trajectories bouncing around unstable fixed points such as the travelling-wave states (TWS) initially discovered by Faisst & Eckhardt (2003) and Wedin & Kerswell (2004) for pipe flow. In linearly stable flows such equilibrium states, known as exact coherent structures (ECS), are disconnected from the laminar flow and are unstable in general (Kerswell & Tutty 2007). The ECS in Waleffe (2001, 2003) and the isolated unstable time-periodic solution in Kawahara & Kida (2001) in PCF are characterized by the same statistics as numerical turbulence. The nonlinear fixed points may thus provide information that could advance the understanding of turbulence, e.g. one could collect and classify these solutions and use them to describe the mean characteristics of a chaotic state. On the other hand, the direct numerical simulations performed by Willis & Kerswell (2008) in pipe flow suggest that other types of solutions, of higher amplitude than those known, are needed in order to describe a fully turbulent flow and that the existing TWS are only related to transitional flows.

The absence of a linear instability mechanisms has previously prevented the discovery of nonlinear solutions to linearly stable canonical flows such as PCF. However, Nagata (1990), for the first time, found time-independent three-dimensional solutions to PCF by first focusing on Taylor–Couette flow between co-rotating cylinders. The solutions to PCF were obtained by bringing down the rotation rate to zero. Later, several nonlinear solutions have been obtained for pipe flow, first by Faisst & Eckhardt (2003) using the idea of a self-sustaining process (SSP) of turbulence proposed by Waleffe (1998), followed by Wedin & Kerswell (2004), Pringle & Kerswell (2007), Duguet, Willis & Kerswell (2008) and Pringle, Duguet & Kerswell (2009).

As far as the rectangular duct flow is concerned, the linear stability study performed by Tatsumi & Yoshimura (1990) shows linear stability up to an aspect ratio of $A = 3.2$ of the rectangular cross-section of the duct. It is only recently that nonlinear solutions for the square duct ($A = 1$) have been discovered by Wedin, Bottaro & Nagata (2009) and Uhlmann, Kawahara & Pinelli (2009) by successfully adopting the SSP approach used in pipe flow. In Wedin *et al.* (2009) it is reported that at transitional conditions the skin friction on the lower branch of the nonlinear solution has a value close to that obtained in direct numerical simulations by Uhlmann *et al.* (2007) and Biau & Bottaro (2009). When the flow speed is sufficiently high, direct numerical simulations of square-duct flow by Gavrilakis (1992), Huser & Biringen (1993), Uhlmann *et al.* (2007) and Biau, Soueid & Bottaro (2008) have all observed an eight-vortex mean flow with two vortices in each quadrant. For example, the study by Gavrilakis (1992) suggests that the secondary Reynolds stress terms cause this mean flow. Recently, Uhlmann & Nagata (2006) performed a linear stability analysis of vertical rectangular duct flow with an internal heat source, finding unstable states for $A = 1$. In this paper we adopt an homotopy approach, alternative to the SSP, by adding the heat equation to the system. A new nonlinear solution to isothermal square duct is discovered by bringing the strength of the heat source to zero.

2. Mathematical formulation

2.1. Configuration and the governing equations

We consider the low-speed motion of a fluid with the kinematic viscosity ν_* , the thermal diffusivity κ_* and the thermal expansion coefficient α_{T*} in a straight duct

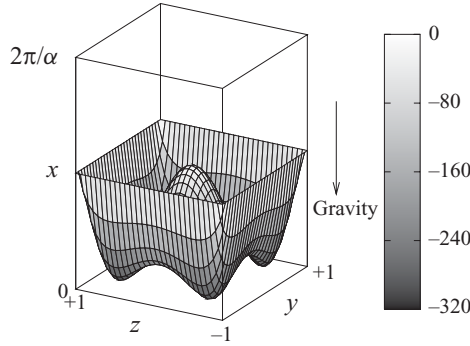


FIGURE 1. The configuration of the model with the basic flow in grey scale at $Re = -3000$ and $Gr = 23000$.

placed vertically in the gravity field. The temperature of all the four vertical walls are kept the same and constant. The cross-section of the duct is a square with the side $2b_*$. The fluid is subject to internal heating which is homogeneously distributed with intensity q_* . We take the Cartesian coordinates with the origin at the centre of the duct. The x_* -axis is directed along the duct and the y_* and z_* -axes are parallel to the sides of the cross-section, as shown in figure 1. Here, the subscript $*$ denotes dimensional quantity. With the Boussinesq approximation, the velocity \mathbf{u} , the pressure P and the temperature deviation T from the wall temperature are governed by the equation of continuity,

$$\nabla \cdot \mathbf{u} = 0, \quad (2.1)$$

the equation of momentum conservation,

$$\partial_t \mathbf{u} + (\mathbf{u} \cdot \nabla) \mathbf{u} = -\nabla P + T \mathbf{e}_x + \nabla^2 \mathbf{u}, \quad (2.2)$$

and the equation of energy conservation,

$$\partial_t T + (\mathbf{u} \cdot \nabla) T = Pr^{-1} (\nabla^2 T + 2Gr), \quad (2.3)$$

where \mathbf{e}_i ($i = x, y, z$) is the unit vector in the i -direction and all the variables have been non-dimensionalized by the length scale b_* , the time scale b_*^2/ν_* , the velocity scale ν_*/b_* and the temperature scale $\nu_*^2/(g_*\alpha_T b_*^3)$, where g_* is the acceleration due to gravity. We have defined the Grashof number as:

$$Gr = \frac{g_* \alpha_T q_* b_*^5}{2\nu_*^2 \kappa_*}, \quad (2.4)$$

and the Prandtl number as:

$$Pr = \frac{\nu_*}{\kappa_*}. \quad (2.5)$$

The electrically conducting aqueous solution of $ZnCl_2$ is often used for internal heating experiments where the heat is released by currents. For 20 wt% aqueous solution of $ZnCl_2$, $Pr = 8.7$ at $20^\circ C$ and $Pr = 6.08$ at $40^\circ C$ (Generalis & Nagata 2003). Throughout this study we fix $Pr = 7$.

The no-slip condition for the velocity and the isothermal condition for the temperature are imposed on the wall:

$$\mathbf{u} = \mathbf{0}, \quad T = 0 \quad \text{at} \quad y = \pm 1 \quad \text{and} \quad z = \pm 1. \quad (2.6)$$

For the x -direction, we impose periodicity over a wavelength of $2\pi/\alpha$.

2.2. *The laminar solution*

The x -independent steady laminar solution, $\mathbf{u} = \mathbf{U}_B = U_B(y, z)\mathbf{e}_x$, $P = P_B = -\chi x$ and $T = T_B(y, z)$, to the governing equations (2.1)–(2.3) with the boundary condition (2.6) obeys

$$0 = \chi + T_B + \Delta_2 U_B, \tag{2.7}$$

$$0 = \Delta_2 T_B + 2Gr, \tag{2.8}$$

$$U_B = T_B = 0 \quad \text{at } y = \pm 1 \quad \text{and } z = \pm 1, \tag{2.9}$$

where χ is the non-dimensional pressure drop and $\Delta_2 \equiv \partial_{yy}^2 + \partial_{zz}^2$. Let $U_{Biso}(y, z)$ be the laminar-velocity field in the isothermal case ($Gr = 0, T_B \equiv 0$) and define the Reynolds number using the centreline velocity:

$$Re = U_{Biso}(0, 0) = \frac{U_{Biso^*}(0, 0)b_*}{\nu_*}. \tag{2.10}$$

Equations (2.7)–(2.9) are solved numerically. The proportionality of the pressure drop to the Reynolds number obeys $\chi = 3.3935Re$ (see Tatsumi & Yoshimura 1990). For the thermal case, the laminar state is classified into five groups depending on the Reynolds number and the Grashof number according to Uhlmann & Nagata (2006). One of the groups, classified in the region M_2 ($-7.69 < Gr/Re < -5.75$) characterizes the flow with the inflection points and no reverse flow, (i.e. $U_B(0, 0) \leq 0$), as shown in figure 1.

2.3. *The disturbance equations*

We superimpose disturbances, $\hat{\mathbf{u}}, \hat{p}$ and $\hat{\theta}$, on the laminar state, $U_B\mathbf{e}_x, P_B$ and T_B , respectively. Disturbances are governed by the following equations:

$$\nabla \cdot \hat{\mathbf{u}} = 0, \tag{2.11}$$

$$\partial_t \hat{\mathbf{u}} + U_B \partial_x \hat{\mathbf{u}} + (\hat{\mathbf{u}} \cdot \nabla) U_B \mathbf{e}_x + (\hat{\mathbf{u}} \cdot \nabla) \hat{\mathbf{u}} = -\nabla \hat{p} + \hat{\theta} \mathbf{e}_x + \nabla^2 \hat{\mathbf{u}}, \tag{2.12}$$

$$\partial_t \hat{\theta} + U_B \partial_x \hat{\theta} + (\hat{\mathbf{u}} \cdot \nabla) T_B + (\hat{\mathbf{u}} \cdot \nabla) \hat{\theta} = Pr^{-1} \nabla^2 \hat{\theta}, \tag{2.13}$$

$$\hat{\mathbf{u}} = \mathbf{0}, \quad \hat{\theta} = 0 \quad \text{at } y = \pm 1 \quad \text{and } z = \pm 1. \tag{2.14}$$

Disturbances $\hat{\mathbf{u}}, \hat{p}, \hat{\theta}$ are decomposed into their mean parts, $\hat{\mathbf{U}}(t, y, z), \hat{P}(t, y, z), \hat{\Theta}(t, y, z)$, and the residuals, $\check{\mathbf{u}}, \check{p}, \check{\theta}$, where $\hat{\mathbf{U}} \equiv \alpha/(2\pi) \int_0^{2\pi/\alpha} \hat{\mathbf{u}} dx = (\hat{U}, \hat{V}, \hat{W}), \hat{P} \equiv \alpha/(2\pi) \int_0^{2\pi/\alpha} \hat{p} dx, \hat{\Theta} \equiv \alpha/(2\pi) \int_0^{2\pi/\alpha} \hat{\theta} dx$, and $\check{\mathbf{u}} = (\check{u}, \check{v}, \check{w})$. We consider the fixed-pressure-gradient constraint so that $\nabla \hat{P} = 0$.

First, we take the streamwise average of (2.11):

$$\partial_y \hat{V} + \partial_z \hat{W} = 0, \tag{2.15}$$

from which the stream function $\hat{\phi}$ of the cross-sectional mean flow (\hat{V}, \hat{W}) can be defined and satisfies

$$\hat{V} = \partial_z \hat{\phi}, \quad \hat{W} = -\partial_y \hat{\phi}. \tag{2.16}$$

Then subtracting (2.15) from (2.11), we obtain $\nabla \cdot \check{\mathbf{u}} = 0$. Solving for $\check{\mathbf{u}}$, we have

$$\check{\mathbf{u}} = -\partial_x^{-1}(\partial_y \check{v} + \partial_z \check{w}), \tag{2.17}$$

where the integrating operator with respect to x , $\partial_x^{-1} \equiv \int dx$, is defined.

In the following, we obtain equations for \hat{U} , $\hat{\phi}$, $\hat{\Theta}$, \check{v} , \check{w} and $\check{\theta}$. Operation of the streamwise average on $\mathbf{e}_x \cdot (2.12)$, $\mathbf{e}_x \cdot \nabla \times (2.12)$ and (2.13) followed by elimination of \hat{V} and \hat{W} by (2.16) leads to

$$\partial_t \hat{U} + (\partial_z \hat{\phi} \partial_y - \partial_y \hat{\phi} \partial_z) \bar{U} - \hat{\Theta} - \Delta_2 \hat{U} + \partial_y \overline{\check{v}\check{v}} + \partial_z \overline{\check{w}\check{w}} = 0, \quad (2.18)$$

$$-(\partial_t + \partial_z \hat{\phi} \partial_y - \partial_y \hat{\phi} \partial_z - \Delta_2) \Delta_2 \hat{\phi} + (\partial_{yy}^2 - \partial_{zz}^2) \overline{\check{v}\check{w}} + \partial_{yz}^2 \overline{\check{w}^2 - \check{v}^2} = 0, \quad (2.19)$$

$$\partial_t \hat{\Theta} + (\partial_z \hat{\phi} \partial_y - \partial_y \hat{\phi} \partial_z) \bar{\Theta} - Pr^{-1} \Delta_2 \hat{\Theta} + \partial_y \overline{\check{v}\check{\theta}} + \partial_z \overline{\check{w}\check{\theta}} = 0, \quad (2.20)$$

where $\overline{\cdot} \equiv \alpha / (2\pi) \int_0^{2\pi/\alpha} \cdot dx$ and \check{u} is given by (2.17). $\bar{U} = U_B + \hat{U}$ and $\bar{\Theta} = T_B + \hat{\Theta}$ are the streamwise mean flow and the mean temperature, respectively.

We eliminate \check{p} by taking the rotation of (2.12). Operation of $\mathbf{e}_z \cdot \nabla \times (2.12)$ and $\mathbf{e}_y \cdot \nabla \times (2.12)$ leads to

$$\begin{aligned} & [\{\partial_t + (\bar{\mathbf{U}} \cdot \nabla) - \nabla^2 + \partial_y \hat{V}\} \partial_x - \partial_{yy}^2 \bar{U}] \check{v} - [\{\partial_t + (\bar{\mathbf{U}} \cdot \nabla) - \nabla^2 + \partial_y \hat{V}\} \partial_y + \partial_y \hat{W} \partial_z] \check{u} \\ & + (\partial_y \bar{U} \partial_z - \partial_z \bar{U} \partial_y - \partial_{yz}^2 \bar{U} + \partial_z \hat{V} \partial_x) \check{w} - (\partial_t - \Delta_2) \partial_y \hat{U} - \partial_y (\hat{\mathbf{U}} \cdot \nabla) \bar{U} \\ & + \partial_y (\hat{\Theta} + \check{\theta}) + \mathbf{e}_z \cdot \nabla \times \{(\check{\mathbf{u}} \cdot \nabla) \check{u}\} = 0, \end{aligned} \quad (2.21)$$

$$\begin{aligned} & [\{\partial_t + (\bar{\mathbf{U}} \cdot \nabla) - \nabla^2 + \partial_z \hat{W}\} \partial_x - \partial_{zz}^2 \bar{U}] \check{w} - [\{\partial_t + (\bar{\mathbf{U}} \cdot \nabla) - \nabla^2 + \partial_z \hat{W}\} \partial_z + \partial_z \hat{V} \partial_y] \check{u} \\ & + (\partial_z \bar{U} \partial_y - \partial_y \bar{U} \partial_z - \partial_{yz}^2 \bar{U} + \partial_y \hat{W} \partial_x) \check{v} - (\partial_t - \Delta_2) \partial_z \hat{U} - \partial_z (\hat{\mathbf{U}} \cdot \nabla) \bar{U} \\ & + \partial_z (\hat{\Theta} + \check{\theta}) - \mathbf{e}_y \cdot \nabla \times \{(\check{\mathbf{u}} \cdot \nabla) \check{u}\} = 0, \end{aligned} \quad (2.22)$$

where $\bar{\mathbf{U}} = (\bar{U}, \hat{V}, \hat{W})$. Subtraction of (2.20) from (2.13) gives

$$\partial_t \check{\theta} + (\bar{\mathbf{U}} \cdot \nabla) \check{\theta} + (\check{\mathbf{u}} \cdot \nabla) \bar{\Theta} + (\check{\mathbf{u}} \cdot \nabla) \check{\theta} - \partial_y \overline{\check{v}\check{\theta}} - \partial_z \overline{\check{w}\check{\theta}} = Pr^{-1} \nabla^2 \check{\theta}. \quad (2.23)$$

In (2.21)–(2.23), \hat{V} , \hat{W} and \check{u} are given by (2.16) and (2.17).

The boundary conditions for \hat{U} , $\hat{\phi}$, $\hat{\Theta}$, \check{v} , \check{w} and $\check{\theta}$ are

$$\hat{U} = \hat{\phi} = \partial_y \hat{\phi} = \partial_z \hat{\phi} = \hat{\Theta} = \check{v} = \check{w} = \partial_y \check{v} = \check{\theta} = 0 \quad \text{at } y = \pm 1, \quad (2.24a)$$

$$\hat{U} = \hat{\phi} = \partial_y \hat{\phi} = \partial_z \hat{\phi} = \hat{\Theta} = \check{v} = \check{w} = \partial_z \check{w} = \check{\theta} = 0 \quad \text{at } z = \pm 1. \quad (2.24b)$$

3. Numerical method

Our method to investigate the linear stability of the flow is exactly the same as the one used by Uhlmann & Nagata (2006). Therefore, only the method for the subsequent nonlinear analysis is presented. We seek a finite-amplitude travelling-wave solution with the streamwise phase velocity, c , so that the residuals, \check{v} , \check{w} and $\check{\theta}$, of the disturbances are expanded as follows:

$$\begin{pmatrix} \check{v} \\ \check{w} \\ \check{\theta} \end{pmatrix} (x, y, z, t) = \sum_{\substack{l=-L \\ l \neq 0}}^L \begin{pmatrix} v_l(y, z) \\ w_l(y, z) \\ \theta_l(y, z) \end{pmatrix} \exp[i l \alpha (x - ct)]. \quad (3.1)$$

Examination of the governing equations (see (2.18)–(2.23)) reveals the following four symmetry groups for the variables, v_l , w_l and θ_l :

$$\text{symmetry I: } v_l \begin{pmatrix} (l^+; e, e) \\ (l^{++}; o, e) \end{pmatrix}, \quad w_l \begin{pmatrix} (l^+; o, o) \\ (l^{++}; e, o) \end{pmatrix}, \quad \theta_l \begin{pmatrix} (l^+; o, e) \\ (l^{++}; e, e) \end{pmatrix}, \quad (3.2a)$$

$$\text{symmetry II: } v_l \begin{pmatrix} (l^+; e, o) \\ (l^{++}; o, e) \end{pmatrix}, \quad w_l \begin{pmatrix} (l^+; o, e) \\ (l^{++}; e, o) \end{pmatrix}, \quad \theta_l \begin{pmatrix} (l^+; o, o) \\ (l^{++}; e, e) \end{pmatrix}, \quad (3.2b)$$

$$\text{symmetry III: } v_l \begin{pmatrix} (l^+; o, e) \\ (l^{++}; o, e) \end{pmatrix}, \quad w_l \begin{pmatrix} (l^+; e, o) \\ (l^{++}; e, o) \end{pmatrix}, \quad \theta_l \begin{pmatrix} (l^+; e, e) \\ (l^{++}; e, e) \end{pmatrix}, \quad (3.2c)$$

$$\text{symmetry IV: } v_l \begin{pmatrix} (l^+; o, o) \\ (l^{++}; o, e) \end{pmatrix}, \quad w_l \begin{pmatrix} (l^+; e, e) \\ (l^{++}; e, o) \end{pmatrix}, \quad \theta_l \begin{pmatrix} (l^+; e, o) \\ (l^{++}; e, e) \end{pmatrix}. \quad (3.2d)$$

Here, l^+ and l^{++} denote odd and even integers, respectively, for l in (3.1). The notation, e or o , implies that the variable is an even or odd function with respect to the y - and z -coordinates. Any of the symmetry groups carries the following symmetry for the mean parts of the disturbance:

$$\hat{U}(e, e), \hat{\varphi}(o, o), \hat{\Theta}(e, e). \quad (3.3)$$

These symmetries are the extension of the four symmetry groups admitted by the linear stability analysis considered by Uhlmann & Nagata (2006). We focus on the symmetry I because it is satisfied by one of the modes which renders the flow unstable according to Uhlmann & Nagata (2006). Note that the symmetries I and IV are equivalent as there is no distinction between y and z in a square duct.

It is easily verified that the symmetry I is composed of the shift-and-reflect symmetry **S** and the mirror symmetry **Z** about the y -axis used by Wedin *et al.* (2009):

$$\mathbf{S} : \begin{pmatrix} u \\ v \\ w \\ \theta \end{pmatrix} (\xi, y, z) \rightarrow \begin{pmatrix} u \\ -v \\ w \\ \theta \end{pmatrix} \left(\xi + \frac{\pi}{\alpha}, -y, z \right), \quad \mathbf{Z} : \begin{pmatrix} u \\ v \\ w \\ \theta \end{pmatrix} (\xi, y, z) \rightarrow \begin{pmatrix} u \\ v \\ -w \\ \theta \end{pmatrix} (\xi, y, -z), \quad (3.4)$$

where $\xi = x - ct$.

All the variables are expanded onto the basis functions ϕ_m and ψ_n as follows:

$$\begin{pmatrix} v_l \\ w_l \\ \theta_l \\ \hat{U} \\ \hat{\varphi} \\ \hat{\Theta} \end{pmatrix} = \sum_{m=1}^M \sum_{n=1}^N \begin{pmatrix} v_{lmn} \phi_m(y) \psi_n(z) \\ w_{lmn} \psi_m(y) \phi_n(z) \\ \theta_{lmn} \psi_m(y) \psi_n(z) \\ U_{mn} \psi_m(y) \psi_n(z) \\ \varphi_{mn} \phi_m(y) \phi_n(z) \\ \Theta_{mn} \psi_m(y) \psi_n(z) \end{pmatrix}, \quad (3.5)$$

where ϕ_m and ψ_n are the combination of the Chebyshev polynomials T_j :

$$\phi_m = \begin{cases} T_{2m} + (m^2 - 1)T_0 - m^2T_2, & \phi_m : e, \\ T_{2m+1} + \frac{m^2 + m - 2}{2}T_1 - \frac{m^2 + m}{2}T_3, & \phi_m : o, \end{cases} \quad (3.6)$$

$$\psi_n = \begin{cases} T_{2n} - T_0, & \psi_n : e, \\ T_{2n+1} - T_1, & \psi_n : o. \end{cases} \quad (3.7)$$

Here, ϕ_m satisfies both the Dirichlet and Neumann conditions, whereas ψ_n satisfies the Dirichlet condition. To have a real solution, the amplitude coefficients, v_{lmn} , etc. in (3.5), must satisfy the reality condition, $v_{lmn}^* = v_{-lmn}$, etc., where * denotes the complex conjugate.

The Galerkin projection of (2.18)–(2.23) with an appropriate truncation gives

$$A_{ij}x_j + B_{ijk}x_jx_k = 0, \quad x_j = (v_{lmn}, w_{lmn}, \theta_{lmn}, U_{mn}, \varphi_{mn}, \Theta_{mn}, c)^T. \quad (3.8)$$

We solve the algebraic equation (3.8) by the Newton–Raphson iterative method. The iteration is continued until the relative errors of all the components of the vector x_j reduce below 10^{-5} .

Following Wedin *et al.* (2009), we adopt the bulk Reynolds number in order to measure the magnitude of nonlinearity, to be compared to the laminar case, where $Re_b = 0.47704Re$:

$$Re_b = \frac{1}{4} \int_{-1}^{+1} \int_{-1}^{+1} \bar{U}(y, z) \, dy \, dz. \quad (3.9)$$

The skin friction λ defined by

$$\lambda = \frac{4\chi}{Re_b^2} \quad (3.10)$$

and the kinetic energy of the flow for one axial period defined by

$$E = \frac{1}{4} \int_{-1}^{+1} \int_{-1}^{+1} \frac{|\mathbf{U}_B + \hat{\mathbf{U}}|^2}{2} \, dy \, dz + \frac{\alpha}{8\pi} \int_0^{2\pi/\alpha} \int_{-1}^{+1} \int_{-1}^{+1} \frac{|\check{\mathbf{u}}|^2}{2} \, dx \, dy \, dz \quad (3.11)$$

also measure the nonlinearity.

4. Results

4.1. The continuation to the isothermal solution

The linear stability analysis shows that the laminar flow becomes unstable to a perturbation with the streamwise wavenumber $\alpha = 1.0$ inside the dashed curve in the Re – Gr plane (see figure 2). This region overlaps the region M_2 for the basic flow classified by Uhlmann & Nagata (2006). In order to establish the continuation of a nonlinear solution in the Re – Gr plane, we first obtain a nonlinear solution with $\alpha = 1.0$ bifurcating from the neutral curve. Our goal is to bring the solution to the isothermal case ($Gr = 0$); one successful continuation path was accomplished by following the arrows, as shown in figure 2. This path is composed of three sections: (a) varying Gr from 17 470 to 30 000 by fixing $Re = -3000$, (b) increasing Re from -3000 to 1000 by fixing $Gr = 30\,000$ and (c) decreasing Gr from 30 000 down to 0 by fixing $Re = 1000$. The amplitude of the solution at each section varies. Accordingly Re_b changes along the path. We plot Re_b at each section in figure 3. In figure 3(a) the path, which starts from the point (black triangle) on the laminar state (dotted curve),

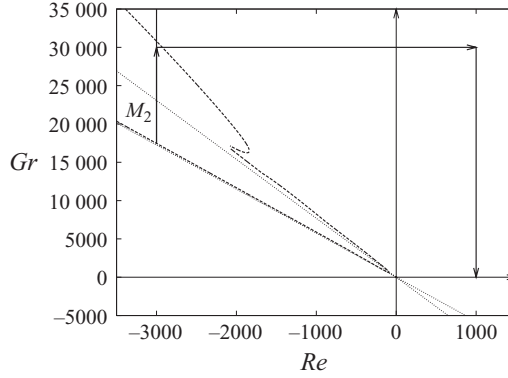


FIGURE 2. The path taken from the linear critical point of the internally heated duct flow to the isothermal solution indicated by the arrows. The dashed curve represents the neutral curve with $\alpha = 1.0$. The region M_2 is bounded by the two thin lines, $Gr/Re = -7.69$ and -5.75 .

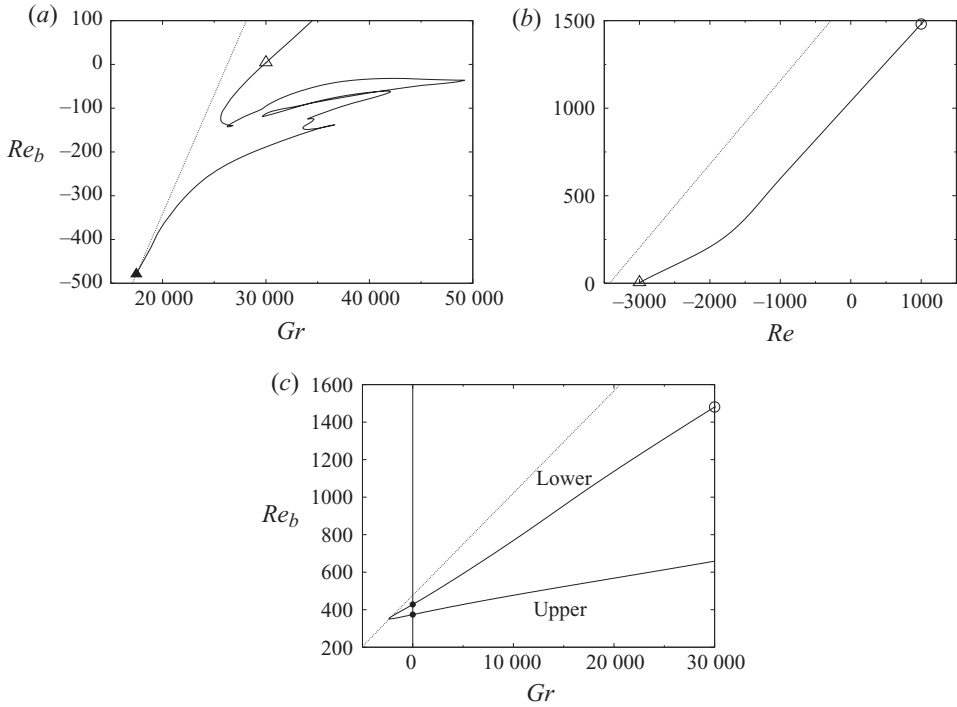


FIGURE 3. The variation of Re_b along the path in figure 2. (a) $Re = -3000$, (b) $Gr = 30000$ and (c) $Re = 1000$. Two closed circles correspond to the isothermal solutions. The dotted line shows the laminar state, $Re_b = 0.47704Re + 0.054480Gr$.

experiences several turning points before it reaches the point $(Gr, Re_b) = (30000, 4.11)$ (open triangle). The path in figure 3(b) continues from the point (open triangle) at $(Gr, Re_b) = (30000, 4.11)$ in figure 3(a). Along the path, Re_b increases monotonically as Re is increased and the path ends at $(Re, Re_b) = (1000, 1481)$ (open circle in figure 3b). As shown in figure 3(c), reducing the Grashof number from 30000 brings the solution to the isothermal case $Gr = 0$ (closed circle on the branch indicated by ‘lower’ in figure 3c). The solution exists even when the Grashof number is decreased

(L, M, N)	c	Re_b	λ
(4, 14, 14)	451.34	331.86	0.10304
(6, 16, 16)	450.54	331.57	0.10322
(8, 18, 18)	450.62	331.60	0.10320
(10, 20, 20)	450.60	331.59	0.10320

TABLE 1. The phase velocity c , the bulk Reynolds number Re_b and the skin friction λ of the upper branch solution with $\alpha = 1.14$ at $Re = 836$ as functions of the truncation level (L, M, N) .

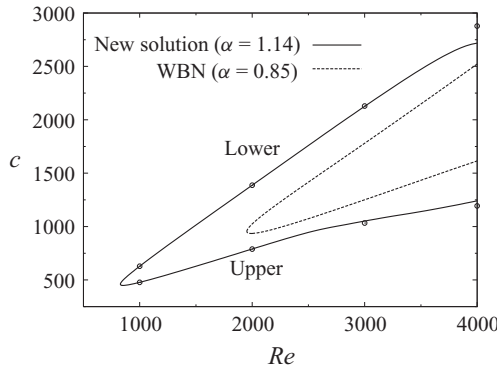


FIGURE 4. The phase velocity c . Solid curve: The new solution. Dotted curve: WBN. The truncation level $(L, M, N) = (6, 16, 16)$ is used to draw the curve, whereas isolated points with $(L, M, N) = (10, 20, 20)$ are plotted with open circles.

further down to -2369 , where the path experiences a turning point. After going around the turning point the path crosses the line, $Gr = 0$, again (another closed circle on the branch indicated by ‘upper’ in the figure) as Gr is increased. We refer to the solution branch closer to the laminar state as the lower branch solution and the solution further away as the upper branch solution, as shown in figure 3(c).

4.2. Travelling wave

The two isothermal solutions (closed circles in figure 3c) are continued in the Re -axis. The nature of the saddle-node bifurcation of these new travelling-wave solution is shown in terms of the phase velocity c in figure 4. The accuracy of the solution close to the saddle-node point with respect to the truncation level is listed in table 1. The solution is seen to converge well at $(L, M, N) = (6, 16, 16)$, which we adopt in the following analysis unless stated otherwise. Also shown in figure 4 is the bifurcation of the travelling-wave solution, referred to as WBN hereafter, obtained by the SSP approach of Wedin *et al.* (2009). The particular wavenumbers indicated in the figure, $\alpha = 1.14$ and 0.85 , correspond to those which give their lowest bulk Reynolds numbers for the present solution and WBN, respectively. These wavenumbers are determined by tracing the existence domain of the solutions in (α, Re_b) space. The domain shrinks as Re is decreased (see figure 5) and we pinpoint the wavenumbers at the saddle-node with the accuracy of the wavenumber increment $\Delta\alpha = 0.01$. The domain of our new travelling-wave solution disappears at $Re = 827.5$.

The kinetic energy E of the flow for one axial period is plotted against Re in figure 6(a), highlighting the proximity of the lower branch state to the laminar solution. A similar effect can be ascertained by inspection of figure 6(b); it is also

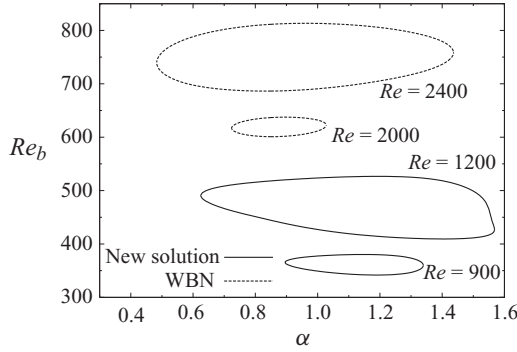


FIGURE 5. The domains of existence of the new travelling-wave solutions (solid curves) and those by WBN (dotted curves).

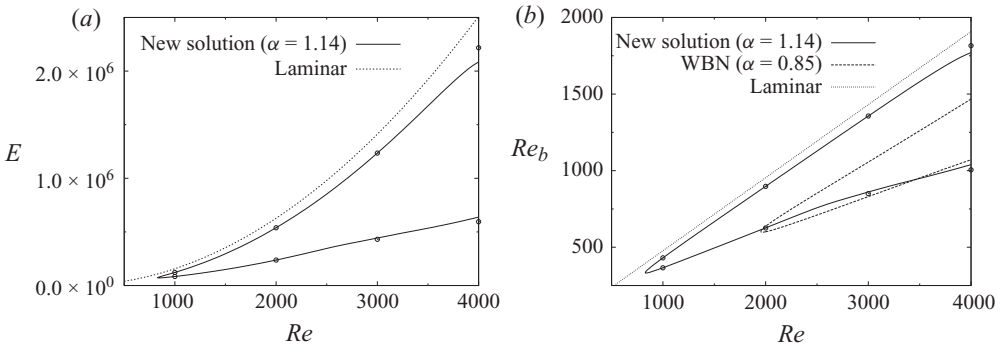


FIGURE 6. (a) Kinetic energy E of the new solution versus Re (solid curve). The dotted curve indicates the energy for the laminar flow given by $1/4 \int_{-1}^1 \int_{-1}^1 U_B^2/2 \, dy \, dz = 0.1568 Re^2$. (b) Bulk Reynolds number versus Re . The truncation level $(L, M, N) = (6, 16, 16)$ is used to draw the curves, and the circles represent isolated solutions with higher truncation, $(L, M, N) = (10, 20, 20)$.

clear that the lower branch of WBN is further away from the laminar state at all values of Re .

Figure 7 shows the skin friction λ against the bulk Reynolds number. In addition to the result of our solution, WBN, the laminar solution and the experimental data of the fully developed turbulence, which obeys $\lambda = 28.45/Re_b$ and $\lambda^{-1/2} = 2 \log_{10}(2.25 Re_b \lambda^{1/2}) - 0.8$ (Jones 1976), respectively, are also plotted. The upper and lower branches of our solution approach the curves given by the experimental data and the laminar flow, respectively, as Re_b is increased. Our solution takes its minimum bulk Reynolds number, 332, at $\alpha = 1.14$, which is substantially smaller than that of WBN (min $Re_b = 598$ at $\alpha = 0.85$).

The iso-surfaces of the streamwise vorticity and the streamwise velocity of the upper branch solution with $\alpha = 1.0$ at $Re = 1500$ are shown in figure 8. Notice the low-speed streak manifested as a wrinkle on the iso-surface of the streamwise velocity in figure 8(b) near the wall at $z = -1$. As can be seen, the low-speed streak is flanked by staggered quasi-streamwise vortices near the walls at $z = \pm 1$. This structure is often identified as the coherent structure of the near-wall turbulence. Figures 9(a) and 10(a) show the mean-flow field, $(U_B + \hat{U}, \hat{V}, \hat{W})$. Both the lower and upper branches display outflow from the wall towards the centre of the duct along $y = 0$. We can

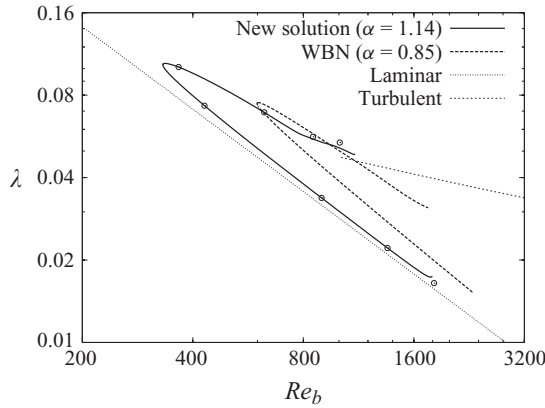


FIGURE 7. The skin friction against the bulk Reynolds number. Solid curve: The current solution. Dashed curve: WBN. $(L, M, N) = (6, 16, 16)$ except for the open circles of the current solution for which $(L, M, N) = (10, 20, 20)$. Dotted line: The laminar flow. Thin dashed curve: The experimental data by Jones (1976).

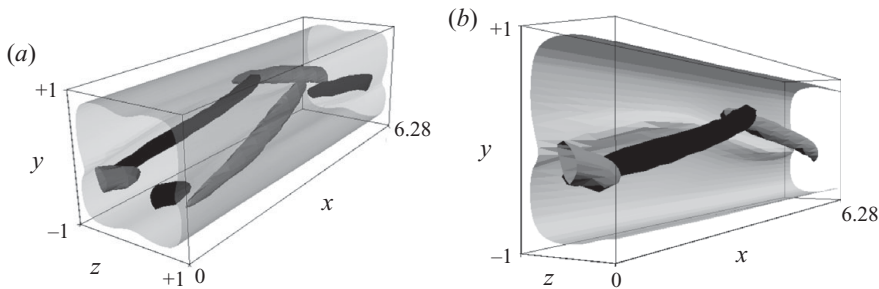


FIGURE 8. The iso-surfaces of the streamwise vorticity and the streamwise velocity of the upper branch solution with $\alpha = 1.0$ at $Re = 1500$ ($Re_b = 506$). Black (dark grey) represents +70% (-70%) of the maximum vorticity and light grey represents 40% of the maximum velocity. (a) The full-flow domain and (b) the close-up of $z < 0$.

also notice three stagnation points in terms of the velocity field (\hat{V}, \hat{W}) on $y = 0$: one at the origin of the axes and the other two approximately half way between the origin and the sidewalls $z = \pm 1$. Also noticeable is the eight-vortex structure (four dominant vortices and four minor vortices): one dominant and one minor vortex in each quadrant. This structure is different from the eight-vortex structure with diagonal symmetry observed in the fully developed turbulence at higher Re (Gavrilakis 1992; Uhlmann *et al.* 2007). The instantaneous total-flow fields are displayed also in figures 9 and 10. The dominant vortices near the walls $z = \pm 1$ oscillate in the y -direction as they propagate in the x -direction (see also figure 8). The minor vortices observed in the mean-flow field are not captured at the vorticity level plotted in figure 8. While the oscillatory motion of the lower branch solution is gentle, the upper branch solution is more active with a vortex oscillating along each of the walls at $z = \pm 1$. According to the DNS result by Uhlmann *et al.* (2007), the marginally turbulent flow ($Re_b \sim 1100$) has a four-vortex structure: two near one of the walls and two more near the wall opposite to it. A similar four-vortex structure has been reported in the DNS by Wedin *et al.* (2008) (see their figure 12). The four-vortex patterns of

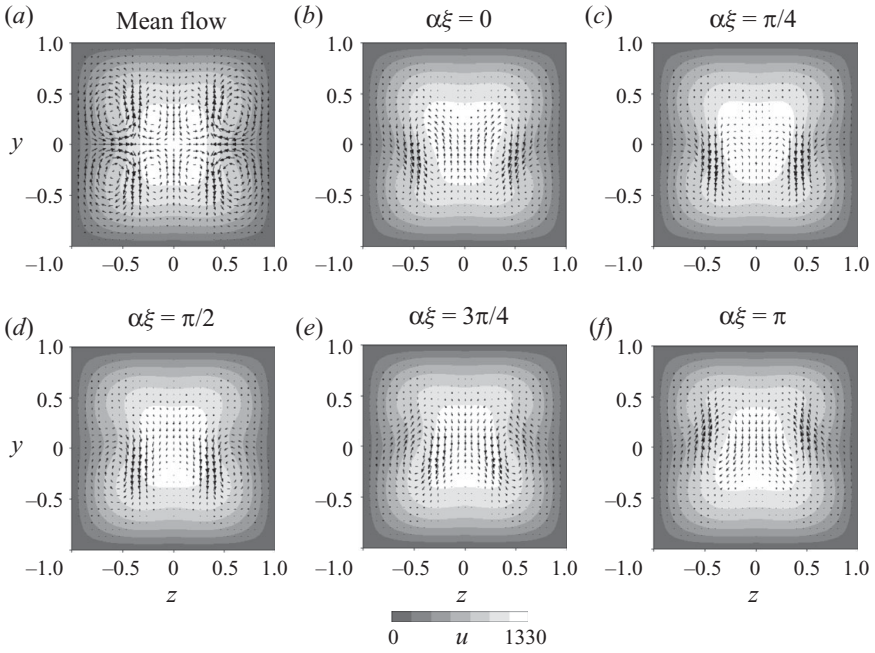


FIGURE 9. Mean flow \bar{U} (a) and images of the total flows $\bar{U} + \check{u}$ along ξ of the lower branch solution with $\alpha = 1.0$ at $Re = 1500$ ($Re_b = 664$). The velocity components are shown on the y - z plane (arrows) and along the x -direction (grey scale). $\xi = x - ct$.

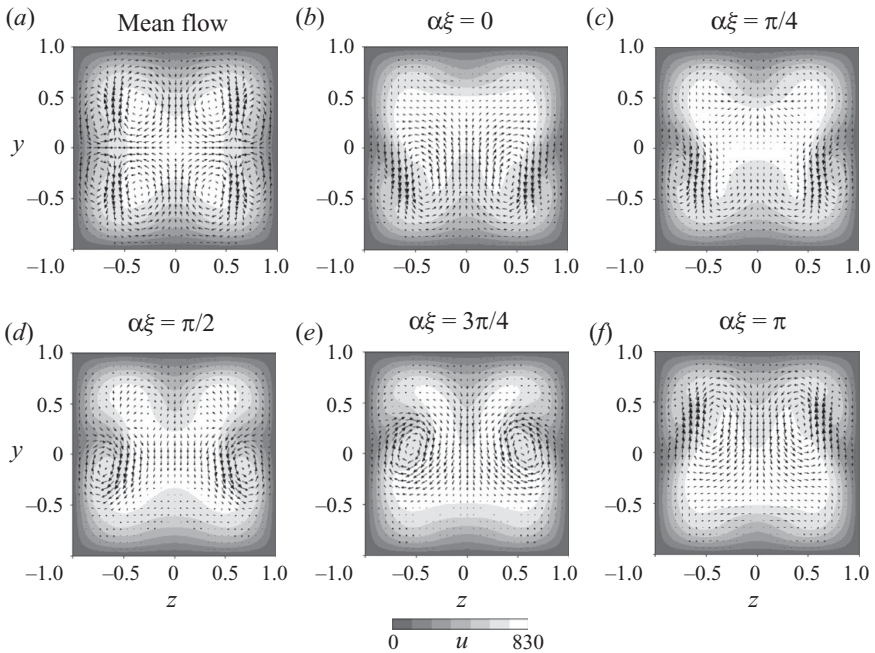


FIGURE 10. Same as figure 9 for the upper branch solution. Here, $Re_b = 506$.

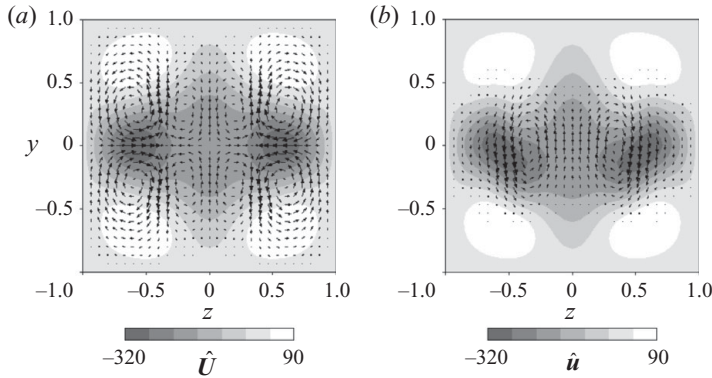


FIGURE 11. The disturbance velocity of the lower branch solution with $\alpha = 1.0$ at $Re = 1500$ ($Re_b = 664$). (a) The mean part \hat{U} and (b) the disturbance \hat{u} at $\alpha\xi = 0$. For the meanings of arrows and grey scale see the caption of figure 9.

Uhlmann *et al.* (2007) have two different orientations, vortices located near $z = \pm 1$ and $y = \pm 1$, that alternate (see their figure 3*a,b*). Biau *et al.* (2008) also observed similar alternating patterns with two pairs of vortices near opposing walls before the flow eventually relaminarises (see their figure 4). In our system, in addition to the solution with four dominant vortices near $z = \pm 1$ displayed in figures 9 and 10, the flow with four vortices near $y = \pm 1$ is also a solution by symmetry.

Figure 11 shows the disturbance velocity field of the lower branch solution. Both the mean part \hat{U} , \hat{V} and \hat{W} and the instantaneous state of the disturbance \hat{u} , \hat{v} and \hat{w} surprisingly resemble those of the mirror-symmetric solution M1 in pipe flow found by Pringle & Kerswell (2007) (see their figure 1). The travelling wave M1 with the axial wavenumber α possesses the shift-and-reflect symmetry, $\mathbf{S} : (u, v, w)(s, \phi, z) \rightarrow (u, -v, w)(s, -\phi, z + \pi/\alpha)$, where (u, v, w) is the velocity components in the cylindrical coordinates (s, ϕ, z) , and the shift-and-rotate symmetry, $\mathbf{\Omega}_m : (u, v, w)(s, \phi, z) \rightarrow (u, v, w)(s, \phi + \pi/m, z + \pi/\alpha)$ with $m = 1$ (Pringle *et al.* 2009). Coupled with the symmetry \mathbf{S} , the symmetry $\mathbf{\Omega}_1$ implies the mirror symmetry, i.e. invariance under reflection in the line $\phi = \pm\pi/2$. For square-duct flow the combined symmetry $\mathbf{S}(\mathbf{Z})$, where \mathbf{S} and \mathbf{Z} are given in (3.4), implies the shift-and-rotate symmetry by the angle π since $\mathbf{S}(\mathbf{Z}) : (u, v, w)(\xi, y, z) \rightarrow \mathbf{S} : (u, v, -w)(\xi, y, -z) \rightarrow (u, -v, -w)(\xi + \pi/\alpha, -y, -z)$. Therefore, the solution in square duct and M1 in pipe flow belong to the same symmetry group. Furthermore, the minimum bulk Reynolds number of our solution, 332 (defined by using the half-width of the side as the length scale), is comparable to their 773 (defined by using the diameter of the pipe as the length scale).

4.3. Stability

In order to investigate the stability of the isothermal travelling-wave solution, $(\mathbf{u}_{TW}, P_{TW})$, found in the previous section, we superimpose infinitesimal perturbations, $(\tilde{\mathbf{u}}, \tilde{P})$, on the solution:

$$\begin{pmatrix} \mathbf{u} \\ P \end{pmatrix} = \begin{pmatrix} \mathbf{u}_{TW} \\ P_{TW} \end{pmatrix} + \begin{pmatrix} \tilde{\mathbf{u}} \\ \tilde{P} \end{pmatrix}. \tag{4.1}$$

Substituting (4.1) into (2.1) and (2.2), we obtain the governing equations for the perturbations:

$$\nabla \cdot \tilde{\mathbf{u}} = 0, \quad (4.2)$$

and

$$\partial_t \tilde{\mathbf{u}} + (\bar{\mathbf{U}} \cdot \nabla) \tilde{\mathbf{u}} + (\tilde{\mathbf{u}} \cdot \nabla) \bar{\mathbf{U}} + (\check{\mathbf{u}} \cdot \nabla) \tilde{\mathbf{u}} + (\tilde{\mathbf{u}} \cdot \nabla) \check{\mathbf{u}} = -\nabla \tilde{P} + \nabla^2 \tilde{\mathbf{u}}, \quad (4.3)$$

where the nonlinear term, $(\tilde{\mathbf{u}} \cdot \nabla) \tilde{\mathbf{u}}$, is neglected. Operating $\mathbf{e}_z \cdot \nabla \times$ and $\mathbf{e}_y \cdot \nabla \times$ on (4.3) leads to

$$\begin{aligned} & [\{\partial_t + (\bar{\mathbf{U}} \cdot \nabla) - \nabla^2 + \partial_y \hat{V}\} \partial_x - \partial_{yy}^2 \bar{U}] \tilde{v} - [\{\partial_t + (\bar{\mathbf{U}} \cdot \nabla) - \nabla^2 + \partial_y \hat{V}\} \partial_y + \partial_y \hat{W} \partial_z] \tilde{u} \\ & + (\partial_y \bar{U} \partial_z - \partial_z \bar{U} \partial_y - \partial_{yz}^2 \bar{U} + \partial_z \hat{V} \partial_x) \tilde{w} + \mathbf{e}_z \cdot \nabla \times \{(\check{\mathbf{u}} \cdot \nabla) \tilde{\mathbf{u}} + (\tilde{\mathbf{u}} \cdot \nabla) \check{\mathbf{u}}\} = 0, \end{aligned} \quad (4.4)$$

$$\begin{aligned} & [\{\partial_t + (\bar{\mathbf{U}} \cdot \nabla) - \nabla^2 + \partial_z \hat{W}\} \partial_x - \partial_{zz}^2 \bar{U}] \tilde{w} - [\{\partial_t + (\bar{\mathbf{U}} \cdot \nabla) - \nabla^2 + \partial_z \hat{W}\} \partial_z + \partial_z \hat{V} \partial_y] \tilde{u} \\ & + (\partial_z \bar{U} \partial_y - \partial_y \bar{U} \partial_z - \partial_{yz}^2 \bar{U} + \partial_y \hat{W} \partial_x) \tilde{v} - \mathbf{e}_y \cdot \nabla \times \{(\check{\mathbf{u}} \cdot \nabla) \tilde{\mathbf{u}} + (\tilde{\mathbf{u}} \cdot \nabla) \check{\mathbf{u}}\} = 0. \end{aligned} \quad (4.5)$$

Based on the Floquet theory, the velocity perturbations, $\tilde{\mathbf{u}}$, is expanded as follows:

$$\tilde{\mathbf{u}}(x, y, z, t) = \sum_{l=-L}^L \tilde{\mathbf{u}}_l \exp[i(l\alpha + d)(x - ct) + \sigma t], \quad (4.6)$$

where σ is the growth rate. We only investigate the fundamental mode ($d=0$) and impose the same symmetries as (3.4) on the perturbations. The interaction of the perturbations $\tilde{\mathbf{u}}$ and the disturbances $\check{\mathbf{u}}$ generates the feedbacks on the mean part. Therefore, we include the x -independent parts $(\tilde{U}, \tilde{V}, \tilde{W}) = (\tilde{u}_0, \tilde{v}_0, \tilde{w}_0) \exp[\sigma t]$ of the perturbations in (4.6) (cf. (3.1)). \tilde{V} and \tilde{W} are derived from the stream function $\tilde{\varphi}$ on the cross-section:

$$\tilde{V} = \partial_z \tilde{\varphi}, \quad \tilde{W} = -\partial_y \tilde{\varphi}. \quad (4.7)$$

Taking the streamwise average of $\mathbf{e}_x \cdot (4.3)$ and $\mathbf{e}_x \cdot \nabla \times (4.3)$ leads to

$$\begin{aligned} & (\partial_t + \partial_z \hat{\varphi} \partial_y - \partial_y \hat{\varphi} \partial_z - \Delta_2) \tilde{U} + (\partial_z \tilde{\varphi} \partial_y - \partial_y \tilde{\varphi} \partial_z) \bar{U} + \partial_y \overline{\tilde{u} \tilde{v}} + \tilde{u} \overline{\tilde{v}} + \partial_z \overline{\tilde{u} \tilde{w}} + \tilde{u} \overline{\tilde{w}} = 0, \quad (4.8) \\ & -(\partial_t + \partial_z \hat{\varphi} \partial_y - \partial_y \hat{\varphi} \partial_z - \Delta_2) \Delta_2 \tilde{\varphi} - (\partial_z \tilde{\varphi} \partial_y - \partial_y \tilde{\varphi} \partial_z) \Delta_2 \hat{\varphi} \\ & + (\partial_{yy}^2 - \partial_{zz}^2) \overline{\tilde{v} \tilde{w}} + \tilde{v} \overline{\tilde{w}} + 2\partial_{yz}^2 \overline{\tilde{w} \tilde{w}} - \tilde{v} \overline{\tilde{v}} = 0, \end{aligned} \quad (4.9)$$

where \tilde{u} is solved by using (4.2), as in (2.17).

The Galerkin projection of (4.4), (4.5), (4.8) and (4.9) gives a generalized eigenvalue problem with the growth rate σ as the eigenvalue,

$$\tilde{A}_{ij} \tilde{x}_j = \sigma \tilde{B}_{ij} \tilde{x}_j, \quad (4.10)$$

where \tilde{x}_j stands for $(\tilde{v}_{lmn}, \tilde{w}_{lmn}, \tilde{u}_{0mn}, \tilde{\varphi}_{0mn})^T$, with $l = -L, \dots, -1, 1, \dots, L$. \tilde{v}_{lmn} , etc. are the amplitude coefficient of \tilde{v}_l , etc. which are expressed in a manner similar to (3.5). The equation is solved by the linear algebra package (LAPACK) routines, ZGESV and ZGEEV.

Figure 12 shows the real part of the growth rate σ of the fundamental mode of the perturbations imposed on the travelling-wave solution with $\alpha = 1.14$. This travelling-wave solution is unstable from its appearance at the saddle-node bifurcation at $Re = 827.5$: while the lower branch has two unstable eigenmodes, the number of unstable eigenmodes increases on the upper branch as the Reynolds number increases. The solution on both branches always presents an eigenmode with zero growth rate,

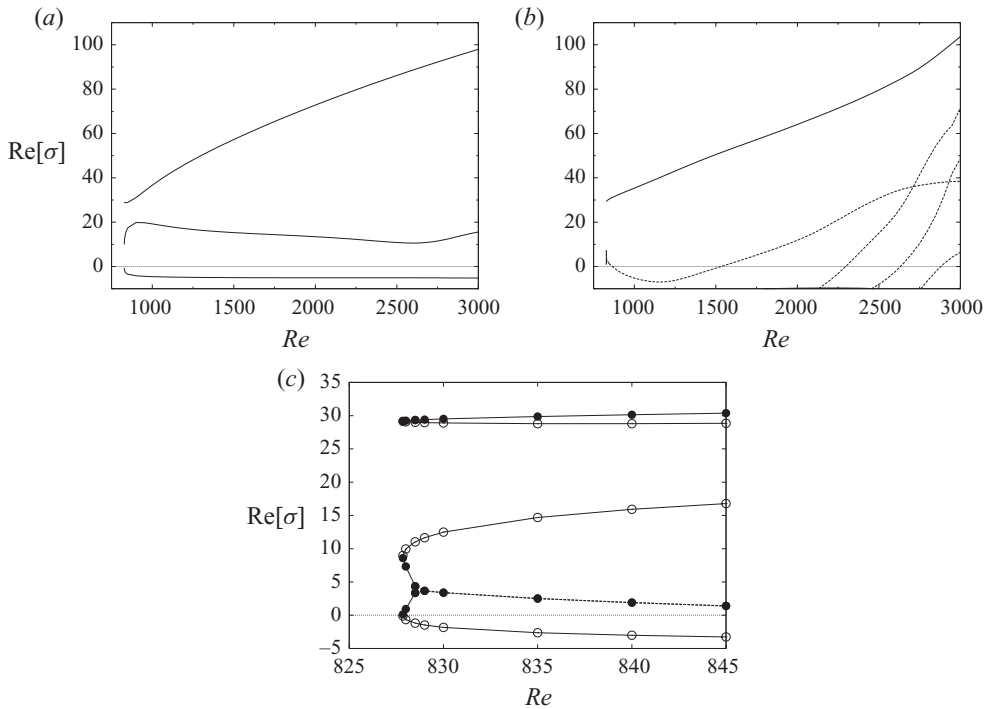


FIGURE 12. The real part of the growth rate, $Re[\sigma]$, of the perturbations to the (a) lower and (b) upper branch solutions with $\alpha = 1.14$. Solid and dotted curves, respectively, indicate that the growth rates are real and complex conjugate. (c) close-up. Curves with open and closed circles correspond to the lower and upper branch, respectively.

which corresponds to the infinitesimal translation in the streamwise direction. The magnified figure (see figure 12c) shows that the growth rates of the upper and lower branches join at the saddle-node. In particular, as expected from the nature of the saddle-node bifurcation, where the upper branch must have one more unstable direction than the lower branch, the third largest real growth rate on the upper branch connects with the third largest (negative) real growth rate of the lower branch at zero. The second and third largest real growth rates on the upper branch near the saddle-node join to become a complex conjugate pair as Re is slightly increased. All the growth rates which cross zero on the upper branch for larger Re are associated with a complex conjugate pair so that time-periodic solutions in the frame moving with the travelling wave are expected to bifurcate there.

The stability analysis for the nonlinear solution with respect to other symmetries and cases with $d \neq 0$ is in progress; however, the results for the fundamental mode reported here are sufficient to demonstrate the instability of the equilibrium solutions identified.

5. Conclusion

The linear stability analysis of internally heated rectangular duct flow by Uhlmann & Nagata (2006) has been extended to the nonlinear case with the special focus on seeking a nonlinear solution in an isothermal case. We have presented a path to achieve

this goal in the $Re-Gr$ plane, starting from the travelling-wave solution bifurcating from the linear critical point of the internally heated flow. The examination of the flow structures and the statistics such as the skin friction obtained so far experimentally (Jones 1976) and numerically (Gavrilakis 1992; Uhlmann *et al.* 2009; Wedin *et al.* 2009) has revealed that our isothermal travelling-wave solution is a new solution. The present disturbance velocity fields exhibit a reflective symmetry about the (mirror) plane $z=0$. This symmetry also holds for the SSP solution by Wedin *et al.* (2009). However, in contrast to the one low-speed streak located near the duct centre in Wedin *et al.* (2009) (see their figure 3), the present solution has two low-speed streaks, one near the wall at $z=1$ and the other at $z=-1$ (see figure 8). Uhlmann *et al.* (2009) use the symmetry II, and therefore their flow structure with four streaks, each on the diagonal of the duct cross-section (see their figure 2), is clearly different from ours which uses the symmetry I. The minimum bulk Reynolds number for the existence of our solution is found to be 332, which is substantially lower than that of the solution found by Wedin *et al.* (2009). The skin frictions of our upper and lower solution branch approach the curves given by the experimental data and the laminar flow, respectively, as Re_b is increased. Comparison with the DNS results of Biau *et al.* (2008) for the flow which lives near the boundary between the laminar and turbulent states seems to suggest that the new solution is embedded in the edge state of the system. The new solution is path independent. However, we could not exclude the possibility of yet other solutions that may exist at the Reynolds number lower than this new solution. Seeking a nonlinear solution which can exist at a smaller Reynolds number is meaningful as it might approach the critical Reynolds number for the global stability of the flow, below which any disturbance eventually decays.

The flow states presented here is the counterpart of the mirror-symmetric solution in pipe flow obtained by Pringle & Kerswell (2007), although the geometries are very different: the rotational symmetry with an arbitrary angle for pipe flow allows for generalization of solutions into larger families than the rotational symmetry with only 90° for square-duct flow.

The stability analysis conducted indicates that the newly found nonlinear solutions are unstable from their onset, thereby rendering their experimental observation tricky. Since neutral points are found for other eigenmodes as Re is increased, further bifurcations of tertiary flows are expected.

H. W. acknowledge the support of a Marie Curie Intra-European Fellowship (PIEF-GA-2008-220201) within the 7th European Community Framework Programme.

REFERENCES

- BIAU, D. & BOTTARO, A. 2009 An optimal path to transition in a duct. *Phil. Trans. R. Soc. A* **367**, 529–544.
- BIAU, D., SOUEID, H. & BOTTARO, A. 2008 Transition to turbulence in duct flow. *J. Fluid Mech.* **596**, 133–142.
- CHAPMAN, S. J. 2002 Subcritical transition in channel flows. *J. Fluid Mech.* **451**, 35–97.
- DARBYSHIRE, A. G. & MULLIN, T. 1995 Transition to turbulence in constant-mass-flux pipe flow. *J. Fluid Mech.* **289**, 83–114.
- DAVEY, A. & DRAZIN, P. G. 1969 The stability of Poiseuille flow in a pipe. *J. Fluid Mech.* **36** (2), 209–218.
- DUGUET, Y., WILLIS, A. P. & KERSWELL, R. R. 2008 Transition in pipe flow: the saddle structure on the boundary of turbulence. *J. Fluid Mech.* **613**, 255–274.
- FAISST, H. & ECKHARDT, B. 2003 Traveling waves in pipe flow. *Phys. Rev. Lett.* **91**, 224–502.

- GAVARINI, M. I., BOTTARO, A. & NIEUWSTADT, F. T. M. 2005 Optimal and robust control of streaks in pipe flow. *J. Fluid Mech.* **537**, 187–219.
- GAVRILAKIS, S. 1992 Numerical simulation of low-Reynolds-number turbulent flow through a straight square duct. *J. Fluid Mech.* **224**, 101–129.
- GENERALIS, S. C. & NAGATA, M. 2003 Transition in homogeneously heated inclined plane parallel shear flows. *J. Heat Trans.* **125**, 795–803.
- HOF, B., JUEL, A. & MULLIN, T. 2003 Scaling of the turbulence transition threshold in a pipe. *Phys. Rev. Lett.* **91**, 244–502.
- HUSER, A. & BIRINGEN, S. 1993 Direct numerical simulation of turbulent flow in a square duct. *J. Fluid Mech.* **257**, 65–95.
- JONES, O. C. 1976 An improvement in the calculation of turbulent friction in rectangular ducts. *ASME J. Fluids Engng* **98**, 173–181.
- KAWAHARA, G. & KIDA, S. 2001 Periodic motion embedded in plane Couette turbulence: regeneration cycle and burst. *J. Fluid Mech.* **449**, 291–300.
- KERSWELL, R. R. & TUTTY, O. R. 2007 Recurrence of travelling waves in transitional pipe flow. *J. Fluid Mech.* **584**, 69–102.
- NAGATA, M. 1990 Three-dimensional finite-amplitude solutions in plane Couette flow: bifurcation from infinity. *J. Fluid Mech.* **217**, 519–527.
- PRINGLE, C. C. T. & KERSWELL, R. R. 2007 Asymmetric, helical and mirror-symmetric travelling waves in pipe flow. *Phys. Rev. Lett.* **99**, 074502.
- PRINGLE, C. C. T., DUGUET, Y. & KERSWELL, R. R. 2009 Highly symmetric travelling waves in pipe flow. *Phil. Trans. R. Soc. A* **367**, 457–472.
- REYNOLDS, O. 1883 An experimental investigation of the circumstances which determine whether the motion of water shall be direct or sinuous and of the law of resistance in parallel channels. *Phil. Trans. R. Soc.* **174**, 935–982.
- TATSUMI, T. & YOSHIMURA, T. 1990 Stability of the laminar flow in a rectangular duct. *J. Fluid Mech.* **212**, 437–449.
- UHLMANN, M. & NAGATA, M. 2006 Linear stability of flow in an internally heated rectangular duct. *J. Fluid Mech.* **551**, 387–404.
- UHLMANN, M., PINELLI, A., KAWAHARA, G. & SEKIMOTO, A. 2007 Marginally turbulent flow in a square duct. *J. Fluid Mech.* **588**, 153–162.
- UHLMANN, M., KAWAHARA, G. & PINELLI, A. 2009 Travelling waves in a straight square duct. In *Advances in Turbulence XII* (ed. B. Eckhardt), In *Proceedings of the 12th European Turbulence Conference*, pp. 585–588. Springer.
- WALEFFE, F. 1998 Three-dimensional coherent states in plane shear flows. *Phys. Rev. Lett.* **81**, 4140–4143.
- WALEFFE, F. 2001 Exact coherent structures in channel flow. *J. Fluid Mech.* **435**, 93–102.
- WALEFFE, F. 2003 Homotopy of exact coherent structures in plane shear flows. *Phys. Fluids* **15**, 1517–1534.
- WALEFFE, F. & WANG, J. 2005 Transition threshold and the self-sustaining process. In *IUTAM Symposium on Laminar–Turbulent Transition and Finite Amplitude Solutions* (ed. T. Mullin & R. Kerswell), pp. 85–106. Springer.
- WEDIN, H. & KERSWELL, R. R. 2004 Exact coherent structures in pipe flow: travelling wave solutions. *J. Fluid Mech.* **508**, 333–371.
- WEDIN, H., BIAU, D., BOTTARO, A. & NAGATA, M. 2008 Coherent flow states in a square duct. *Phys. Fluids* **20**, 094105.
- WEDIN, H., BOTTARO, A. & NAGATA, M. 2009 Three-dimensional traveling waves in a square duct. *Phys. Rev. E* **79**, 065305.
- WILLIS, A. P. & KERSWELL, R. R. 2008 Coherent structures in localized and global pipe turbulence. *Phys. Rev. Lett.* **100**, 124501.